



Improved Suzuki–Miyaura reaction conversion efficiency using magnetic nanoparticles and inductive heating

Alejandro Villacampa¹, Luis Duque¹, Olga Juanes², Francisco Javier Palomares³, Pilar Herrasti¹, and Nieves Menéndez^{1,*} 

¹Departamento de Química Física Aplicada, Facultad de Ciencias, Universidad Autónoma de Madrid, Cantoblanco, Madrid, Spain

²Departamento de Química Orgánica, Facultad de Ciencias, Universidad Autónoma de Madrid, Cantoblanco, Madrid, Spain

³Instituto de Ciencia de Materiales de Madrid (ICMM), Consejo Superior de Investigaciones Científicas (CSIC), Cantoblanco, Madrid, Spain

Received: 6 May 2021

Accepted: 25 September 2021

Published online:

3 January 2022

© The Author(s) 2021

ABSTRACT

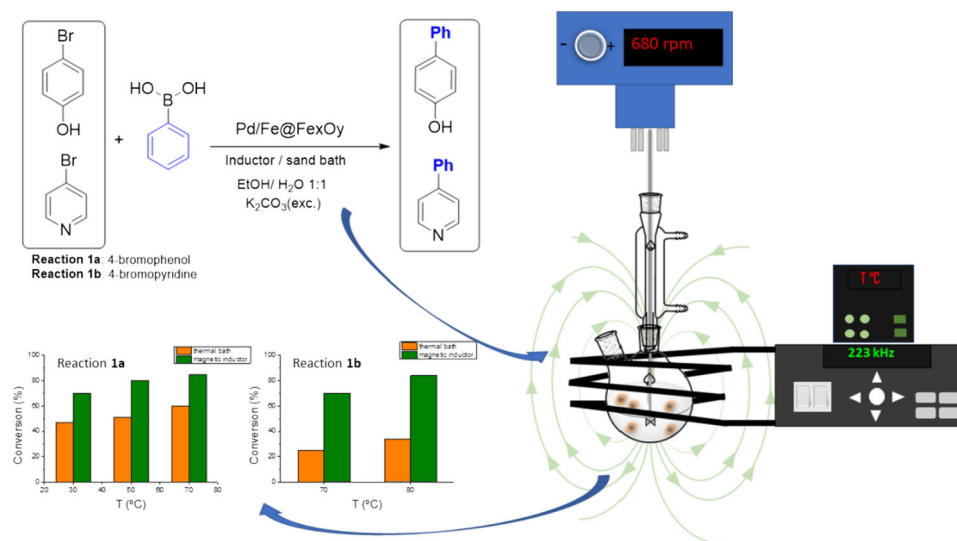
The use of magnetic nanoparticles in C–C coupling reactions enables the facile recovery of the catalyst under environmentally friendly conditions. Herein, the synthesis of Pd/Fe@Fe₃O₄ nanoparticles by the reduction of Pd²⁺ and oxidation of Fe on the surface of preformed Fe@Fe₃O₄ is reported. The nanoparticles were characterized using a variety of analytical techniques (transmission electron microscopy, Mössbauer spectroscopy, X-ray photoelectron spectroscopy, and X-ray diffraction) to determine their size, structure, and chemical composition. The catalytic efficiency of these nanoparticles in classical Suzuki–Miyaura coupling reactions was investigated. The nanoparticles achieved high catalytic activity with the application of local heating by an alternating magnetic field. An investigation was conducted at identical temperatures to compare global heating with the application of an external magnetic field; magnetic heating demonstrated excellent substrate conversion in lesser time and at a lower temperature. The catalyst could also be recycled and reused three times, with ~ 30% decrease in the substrate conversion, which is most likely due to the agglomeration of the Pd nanoparticles or poisoning of the Pd catalyst. This approach, which takes advantage of the catalytic activity and magnetic susceptibility of magnetic nanoparticles, can be applied to several organic transformations to improve their efficiency.

Handling Editor: Dale Huber.

Address correspondence to E-mail: nieves.menendez@uam.es

<https://doi.org/10.1007/s10853-021-06591-w>

GRAPHICAL ABSTRACT



Introduction

The use of transition metal compounds containing elements such as Pd, Au, Ni, Cu, and Ru to catalyze different organic reactions is well known [1–7]. The Suzuki–Miyaura reaction, a reaction between a halogenated hydrocarbon and an arylboronic acid, was first reported in 1979 [8] and is widely used as a route to synthesize C–C bonds. It is mainly catalyzed by Pd owing to its high activity and selectivity and is one of the most widely accepted methods for the synthesis of pharmaceuticals [9]. The advantages of the Suzuki–Miyaura reaction include tolerance to aqueous media, functional group diversity and tolerance, high conversions, and mild reaction conditions.

Traditional reactions using homogeneous Pd complexes as catalysts have been described [10, 11]. The complexes exhibited high performance and stereoselectivity, but the formation of insoluble Pd black or aggregation of the insoluble species diminished its catalytic activity in the coupling reaction [12, 13]. In addition, it is very difficult to recycle and recover homogeneous catalysts as they remain in the reaction medium at low concentrations and cannot be separated from the synthesis product, which increases the

cost of the process and potentially results in catalyst unavailability and product impurity [14]. Therefore, it is necessary to design economical and efficient environmental processes for the separation and reuse of catalysts. This approach has attracted enormous attention in the twenty-first century.

Using a heterogeneous catalyst can efficiently solve these problems and facilitate easy separation of the catalyst from the reaction mixture [15]. Pd has been immobilized on silica nanoparticles [16, 17], graphene [18], carbon nanotubes [19], metal–organic frameworks [20, 21], and metal oxides [22, 23]; however, these catalysts are expensive and usually require complicated and tedious preparation procedures. To overcome these drawbacks, the development of practical, economical, and environmentally friendly supported Pd catalysts is required.

The anchoring of catalysts to magnetic nanoparticles (MNPs) has been extensively studied in the recent years [24–26]. Iron oxide nanoparticles exhibit many advantages, including a high surface-to-volume ratio and facile magnetic recovery [27]. The magnetically recoverable catalyst has attracted significant attention because its recovery process is more economical and greener compared to centrifugation and filtration. Magnetite is one of the most commonly used metal oxide nanoparticles owing to its magnetic

properties and biocompatibility. Pd-functionalized magnetite nanoparticles have been reported for application in the Suzuki–Miyaura reaction [16, 22, 28]. In general, the functionalization process involves difficult and time-consuming ligand synthesis and additional costs. To minimize the use of ligands in the Pd incorporation process, facile procedures based on sequestering processes were studied on materials capable of reducing Pd by oxidizing the surface of the sequestering material. Li et al. studied the sequestration of Ni(II) in a solution using Fe nanoparticles [29]. The process involved coordination of the metal ion to the surface of the reactive Fe, which acts as a reductant toward the less reactive metal ions. Applying this concept, $\text{Fe}_x\text{O}_y@Fe$ was synthesized to recover a variety of ions, such as Co^{2+} , Cu^{2+} , Ni^{2+} , Rh^{3+} , Pd^{2+} , Ag^+ , and Pt^{4+} , from solution [30, 31].

The use of heterogeneous catalysts in the Suzuki–Miyaura reaction requires relatively elevated reaction temperatures, which can be achieved using a local heating procedure. The magnetic properties of magnetite nanoparticles enable the conversion of electromagnetic induction (EMI) into heat. The use of induction heating offers remarkable benefits compared with other heating methods, such as microwave irradiation and thermal baths, owing to the penetration power of the magnetic field [32]. In addition, EMI can quickly and directly induce high temperatures in catalyst particles [33, 34]. Thus, heating the system by EMI takes less time compared with external heating methods that involve a conventional heat source, such as a thermal bath, and provides greater control and safety over the reaction. The application of PEG- or oleic-acid-coated $\text{Fe}@Fe_3O_4$ nanoparticles with Pd adsorbed on the surface in Suzuki–Miyaura and Sonogashira reactions has been reported recently, demonstrating the feasibility of this approach [35]. Our study demonstrates the novel use of uncoated $\text{Pd}/\text{Fe}@Fe_3O_4$ nanoparticles with excellent catalytic activity in the Suzuki–Miyaura reaction heating by EMI. Nanoparticles are usually coated to prevent agglomeration and loss of their electrical and magnetic properties; however, we show that vigorous agitation does not result in a loss of properties, making it possible to apply lower frequency magnetic fields than those required for coated nanoparticles. The effect of different heat sources and temperatures on the efficiency of the heterogeneous catalytic Suzuki–Miyaura reaction was analyzed, and

the results indicated that inductive heating improved the catalyst efficiency. The recovery and reuse of the catalysts was also tested.

Experimental section

Catalyst synthesis

The catalyst was prepared in two stages according to a previously reported procedure [31, 36]. Briefly, a solution of NaBH_4 (2.24 g, 59 mmol) in 30 mL of deionized (DI) water was added dropwise (for a period of approximately 15 min) to a solution of $\text{FeCl}_3 \cdot 6\text{H}_2\text{O}$ (5.67 g, 21 mmol) in DI water (400 mL). The mixture was mechanically stirred at 600 rpm for 4 h, to form a black precipitate. The nanoparticles were separated using a magnet, and the supernatant was discarded. The solid was washed and sonicated with DI water three times, and finally with ethanol to produce a transparent solution. Finally, the resulting black paste was centrifuged and vacuum-dried overnight at 25 °C to yield $\text{Fe}@Fe_xO_y$ powder (1 g). In the second stage, to obtain the $\text{Pd}/\text{Fe}@Fe_xO_y$ catalyst, 200 mg of $\text{Fe}@Fe_xO_y$ was reacted with $\text{Pd}(\text{NO}_3)_2$ (230 mg, 1 mmol) of in 250 mL of DI water at a pH of 10.5 under an argon atmosphere. The mixture was sonicated for 4 h increasing the temperature to 45–50 °C. The reaction mixture was subsequently centrifuged for 10 min at 10000 rpm, and the black precipitate was washed with distilled water several times, followed by vacuum drying for 12 h at 25 °C. The synthesis and purification steps were carried out in air, although the catalyst was stored in an inert atmosphere to prevent oxidation over time.

Material characterization

Phase identification analysis of the MNPs was conducted by X-ray diffraction (XRD) using a Bruker D8 powder diffractometer equipped with a primary monochromator and an ultrafast Lynxeye XE-T multichannel detector with $\text{Cu K}\alpha_1$ radiation. The patterns were collected in the 2θ range of 5–80°, with an angular increment of 0.02° and an increment time of 1 s. The diffractograms were analyzed using the PANalytical *X'Pert HighScore* program, and their profile fitting was carried out to obtain more reliable peak parameters after deconvolution of the overlapped peaks. Peaks were assigned based on the

International Center for Diffraction Data (ICDD) reference considering the peak positions and intensities. A semiquantitative XRD analysis of the composition based on the reference intensity ratio (RIR) was also performed. The morphology of the catalyst was studied using a transmission electron microscope (JEOL JEM 1010) operated at 100 kV. The samples were prepared by placing a single droplet (10 μL) of an aqueous solution of MNPs onto a copper grid coated with a carbon film. The grid was dried in air for several hours at room temperature (RT). Mössbauer spectroscopy was used to analyze the Fe phases in the samples. The spectra were recorded at RT in the triangular mode using a transmission spectrometer with a $^{57}\text{Co}/\text{Rh}$ source. Spectral analyses were performed by nonlinear fitting using the NORMOS program [37]. Each spectrum was fitted by the convolution of subspectra corresponding to as many different crystallographic positions of Fe that could be identified in the material by XRD. For each Fe site, the isomer shift (δ), quadrupole splitting (ΔE_Q), and hyperfine magnetic field (H) were fitted. We fixed equal full width at half maximum of the Lorentzian lines of each component, and the intensity ratio 3:2:1:1:2:3 for each sextet. The combination of these three parameters allows for the identification of a particular compound. The energy calibrations were performed using an $\alpha\text{-Fe}$ (6 μm) foil. The composition of the material was also examined by inductively coupled plasma optical emission spectroscopy (ICP-OES) using a Perkin-Elmer Optima 2100 DV system to determine the Pd loading on the catalyst before and after its use and the possible leaching of Fe and/or Pd; each sample was analyzed three times. X-ray photoelectron spectroscopy (XPS) was used to characterize the surface chemistry of the samples and the oxidation states of Fe and Pd. XPS experiments were performed in a UHV chamber with a base pressure of 10^{-10} mbar equipped with a hemispherical electron energy analyzer (SPECS Phoibos 150 spectrometer) and a 2D delay-line detector (Surface Concept), using a non-monochromatic X-ray source of Al $K\alpha$ radiation (1486.6 eV) operated at 300 W. XPS spectra were recorded at the normal emission take-off angle, using an energy step of 0.50 and 0.10 eV and a pass-energy of 40 and 20 eV for survey spectra and detailed core-level regions (Fe 2p, Pd 3d, C 1s, Fe 3p, Pd 4p, and O 1s), respectively. The charging effects accumulated in the photoemission process were compensated using a low energy electron flood gun, in which a

wide beam illuminates the sample surface during the measurements. On the one hand, this allows the binding energy calibration to be referenced to the C 1s photoelectron peak at 284.5 eV, which was checked before and after the measurement of every selected core-level transition. On the other hand, and more importantly, charge compensation also provides the correct lineshape of a given core-level emission, which is significantly affected in the absence of flood-gun irradiation and unfortunately leads to contradictory conclusions in the determination of the oxidation states present. Data processing was performed using CasaXPS software (Casa Software Ltd., Cheshire, UK). Spectra are displayed after the subtraction of the contribution of the Al- $K\alpha$ satellite emission; in some cases, the spectra were normalized to the maximum intensity to highlight the lineshape differences, which provides direct valuable insight into the oxidation states. $^1\text{H-NMR}$ spectroscopy was performed on a Bruker Avance 300 MHz instrument to determine the conversion of the Suzuki–Miyaura reactions. To calculate the conversion, each $^1\text{H-NMR}$ spectrum was integrated relative to the internal standard 1,3,5-trimethoxybenzene. The samples were prepared by dissolving 0.2 mL of the crude reaction in 0.4 mL of deuterated dimethylsulfoxide ($\text{DMSO-}d_6$).

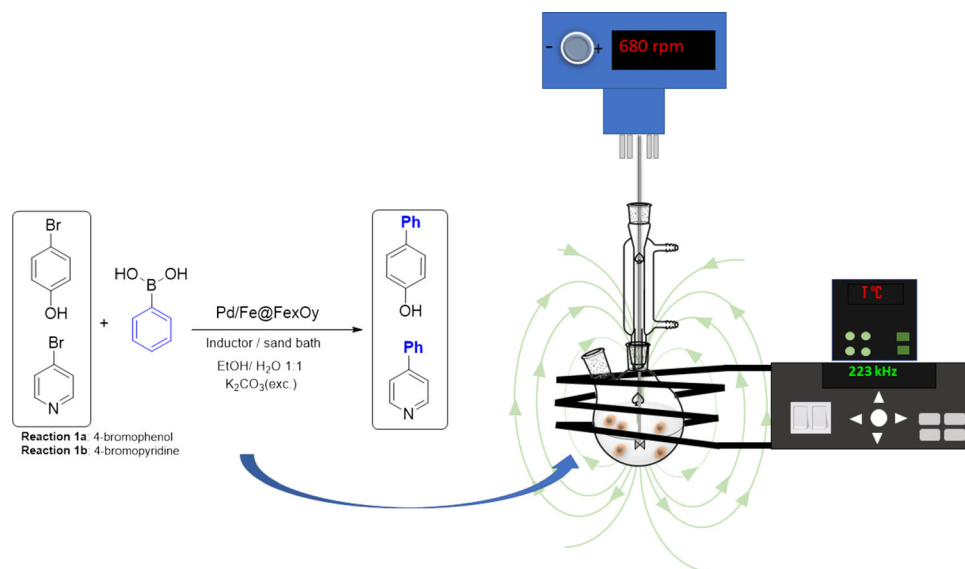
Suzuki–Miyaura coupling reactions

The efficiency of the Pd/Fe@Fe₃O₄ catalyst under magnetic induction heating was tested in the catalyzed coupling of phenylboronic acid with 4-bromophenol and 4-bromopyridine. The conversions of both reactions were compared using two heating sources: a conventional thermal bath and an alternating magnetic field. A schematic of the reactions and the magnetic system is shown in Fig. 1.

For reaction **1a**, 4-bromophenol (1.8 mmol), phenylboronic acid (2.7 mmol), and 1,3,5-trimethoxybenzene (1.8 mmol) as an internal standard were dissolved in 5 mL of ethanol. K₂CO₃ (3.6 mmol) was dissolved in 5 mL of DI water and added to the mixture with 30 mg of Pd/Fe@Fe_xO_y (5 mol% Pd). The reaction mixtures were mechanically stirred in a glass reactor in air over the required reaction times.

For reaction **1b**, 4-bromopyridine hydrochloride (1.8 mmol), phenylboronic acid (2.7 mmol), and 1,3,5-trimethoxybenzene (1.8 mmol) were dissolved in 5 mL of ethanol. K₂CO₃ (7.2 mmol) because

Figure 1 Schematic of the Suzuki–Miyaura reaction conducted under induction heating.



4-bromopyridine was added as hydrochloride) was dissolved in 5 mL of DI water and added to the mixture with 30 mg of Pd/Fe@Fe_xO_y (5 mol% Pd). The reaction mixture was treated as described in reaction 1a.

The conversions of the reactions were determined over time by comparing the concentrations of the final products through ¹H-NMR analysis at the start of the reactions and after different reaction times. Some of these ¹H-NMR spectra are provide in the Supplementary Information.

Magnetic induction heating was performed using an electromagnetic coil of an EASYHEAT LI 8310 apparatus (Ambrell) equipped with a water-cooling system. The fourth-turn coil diameter was 7.5 cm with a depth of 4.5 cm. Alternating currents between 200 and 550 A were applied at a constant frequency of 223 kHz to reach the desired temperature in the reaction medium (see Supplementary Information). A temperature signal was supplied to a temperature controller (Yokogawa) that could regulate the intensity of the alternating current flowing through the magnetic inductor coil to maintain the reaction at a constant temperature. The reaction temperature was measured using an optical fiber.

Results and discussion

Catalyst characterization

To obtain the Pd catalyst, an Fe@Fe₃O₄ solid support was fabricated, which acted as a reducing agent for the Pd²⁺ solution and resulted in its attachment to the surface. Figure 2 shows a characteristic X-ray diffractogram of the Fe@Fe₃O₄ precursor. All diffraction peaks match the standard JCPDS no. 01-087-0722, 01-089-2355 and 01-075-1594, which correspond to Fe, Fe₃O₄, and FeOOH, respectively. Figure 2 shows the positions of the Bragg peaks of the phases present as well as the difference between the observed and calculated patterns. Semiquantitative XRD analysis revealed the formation of 42 wt.% zerovalent Fe, 37 wt.% Fe₃O₄, and 21 wt.% FeOOH.

Transmission electron microscopy (TEM) analysis of Fe@Fe₃O₄ (Fig. 3a) shows the formation of two types of nanoparticles. The larger particles have sizes of 20–100 nm and correspond to Fe and Fe₃O₄; these particles have a cuboid appearance and form aggregated, cross-linked chains owing to their magnetic nature (Figure S1, Supplementary Information) [30]. The smaller particles (with sizes less than 10 nm) would correspond to Fe(0) and are distributed over the surface of the Fe@Fe₃O₄ (indicated by arrows in Fig. 3a). XPS was used to analyze the surface of the material in detail and corroborate this hypothesis, as the previously reported results indicate the formation of an amorphous iron core and a shell formed mostly by Fe₃O₄ and FeOOH [31, 36]. Figure 3b shows the Fe

Figure 2 XRD diffractogram of Fe@Fe₃O₄. The observed, calculated, and difference patterns are shown. Semiquantitative XRD analysis and the Bragg positions of the phases present are included.

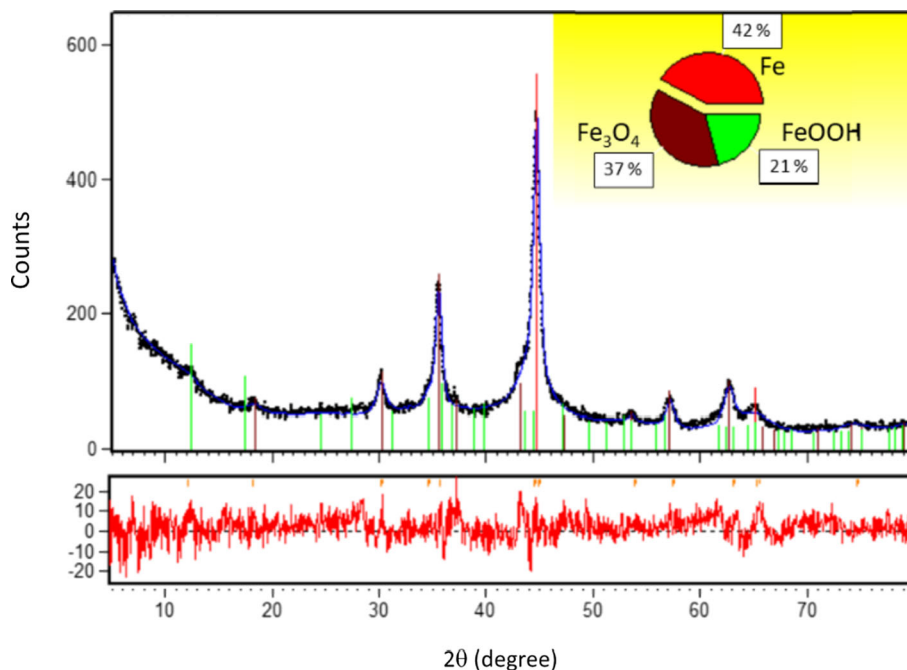
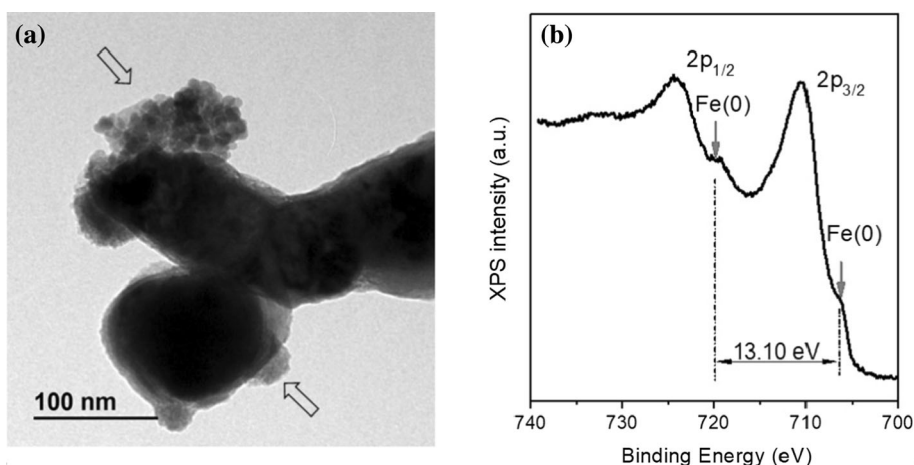


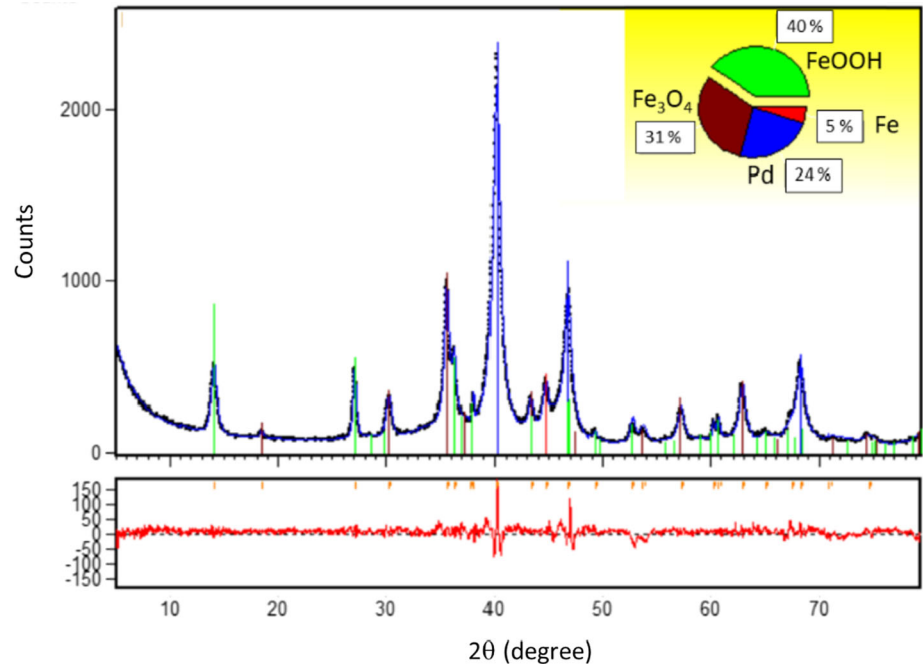
Figure 3 **a** TEM micrograph and **b** Fe2p XPS (Al-Kα) spectrum of Fe@Fe₃O₄.



2p core-level emission corresponding to the Fe@Fe₃O₄ sample. The XPS spectrum shows the photoelectron emission of the complex lineshape mainly dominated by two wide peaks corresponding to the spin-orbit 3/2 and 1/2 doublet. The oxidation states can be determined by comparing the binding energy positions of both peaks, their energy splitting, and the presence/absence of characteristic satellites, in comparison with pure iron and standard iron oxide compounds [38, 39]. In our case, the analysis of the multiplet structure only reveals a very weak emission above the 2p_{1/2} component and a negligible signal between the doublet; it is noteworthy that the emission at lower binding energy comes from Fe(0), as

discussed below. In accordance with this result, together with the binding energy values of 2p_{3/2} (710.2 eV) and splitting (13.6 eV), we suggest that the surface oxide signal arises mainly from Fe₃O₄. In addition, from the detailed analysis of the spectral lineshape, a prominent emission at 706.7 eV (arrow on the right in the figure) significantly shifted to a lower binding energy than the oxide can be observed. According to this binding energy value, the signal can be attributed to 2p_{3/2} from zerovalent Fe, which also has its spin-orbit counterpart (arrow on the left of the figure) shifted by 13.10 eV. Therefore, the presence of both components and the characteristic splitting provides a straightforward confirmation of

Figure 4 XRD diffractogram of Pd/Fe@Fe₃O₄. The observed (dots), calculated (blue line) and difference patterns are shown. Semiquantitative XRD analysis and the Bragg positions of the phases present are included.



the existence of a significant amount of Fe(0) in the sample surface.

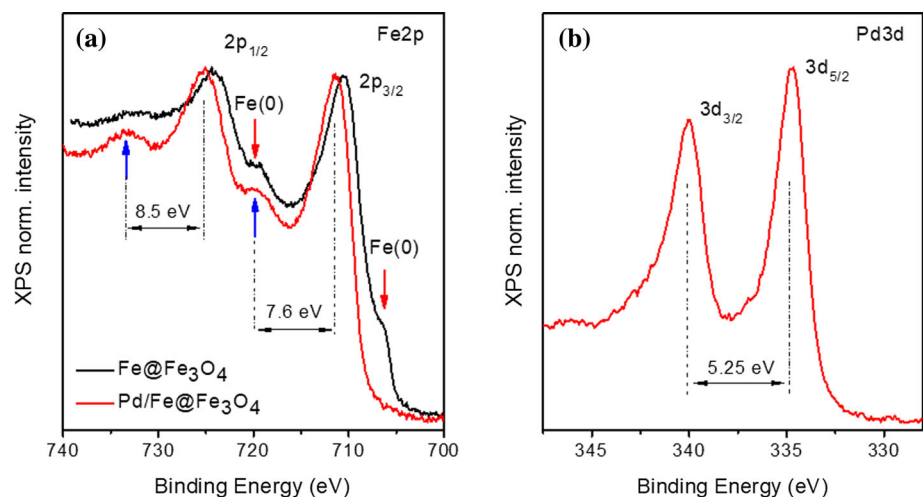
Fe@Fe₃O₄ can act as a reducing agent, which adsorbs and reduces Pd²⁺ to zerovalent Pd during the synthesis process. Figure 4 shows the diffractogram obtained for the Pd/Fe@Fe₃O₄ sample, in which peaks corresponding to Fe, Fe₃O₄, FeOOH, and Pd (JCPDS no. 03-065-6174) are observed, demonstrating the successful anchoring of Pd to the substrate. Semiquantitative XRD analysis indicated that the sample contained 24 wt.% Pd, 5 wt.% Fe, 40 wt.% FeOOH, and 31 wt.% Fe₃O₄. The amount of Pd determined through semiquantitative analysis

corresponded with ICP-OES results obtained for the digested Pd/Fe@Fe₃O₄ sample (35 ± 1 wt.% Pd).

The Pd/Fe@Fe₃O₄ TEM image (Figure S2) shows an increase in needle-like structures that are characteristic of FeOOH [40]. In addition, larger particles, probably corresponding to Fe₃O₄, and darker particles of Pd and Fe are also shown.

Figure 5a displays the normalized Fe 2p spectra of Fe@Fe₃O₄ and Pd/Fe@Fe₃O₄. Upon comparison, important lineshape differences can be observed clearly. First, the characteristic emission of Fe(0) is missing on the surface of the Pd/Fe@Fe₃O₄ sample. Second, there is a shift to higher binding energy values for both 2p_{3/2} and 2p_{1/2} oxide peaks, which is

Figure 5 XPS (Al-Kα) spectra: **a** normalized Fe 2p spectra of Fe@Fe₃O₄ and Pd/Fe@Fe₃O₄ **b** Pd 3d core level of Pd/Fe@Fe₃O₄.



tentatively indicative of Fe^{3+} enrichment. In addition, a multiplet structure appears at higher energy values for each doublet peak. Following a similar analysis to that of Fig. 3b, the separation between the satellites and main peaks, 7.6 and 8.5 eV, respectively, is consistent with the majority presence of Fe^{3+} , which can be understood as additional FeO–OH bonds present on the surface of this sample [39]. This result agrees with the increased emission of the OH component in the O 1s core-level spectrum located at higher energy values from the signal ascribed to oxygen in the metallic oxide lattice (not showed). Figure 5b shows the XPS data of the Pd 3d core-level of Pd/Fe@Fe₃O₄. In contrast to the Fe species, the Pd 3d spectrum is basically composed of the well-defined and narrow 3d_{5/2} and 3d_{3/2} peaks, located at the right binding energy of 334.8 eV and with an energy splitting of 5.25 eV, ascribed to Pd(0) [36]. Note that there exists a subtle emission on the higher-energy side of the doublet owing to the residual formation of native oxide due to air exposure of the sample prior to XPS measurements. Therefore, a chemical reduction from Pd²⁺ to Pd(0) occurred during the synthesis of Pd/Fe@Fe₃O₄.

The Mössbauer spectra of the catalyst and support, obtained at different stages of the synthetic process, are shown in Fig. 6. The Fe@Fe₃O₄ spectrum was fitted by overlapping a central doublet (with $\delta = 0.36$ mm/s and $\Delta E_Q = 0.7$ mm/s) and a sextet (with $\delta = 0.02$ mm/s, $\Delta E_Q = 0.0$ mm/s and $H = 33.1$ T), corresponding to FeOOH and Fe(0) detected by XRD, respectively. In addition, a broad sextet, corresponding to the Fe₃O₄ phase according to the XRD results, was also present. This subspectrum was fitted as a hyperfine field distribution (inset in Fig. 6a) that reflects the randomness of the environment of the Fe atoms owing to the wide size distribution of the nanoparticles or poor crystallinity. The

most probable hyperfine magnetic field value is 25.2 T, which is much lower than values corresponding to bulk-sized magnetite. The spectrum of bulk-sized magnetite is formed by two sextets, of 45 and 49 T, which correspond to Fe in the tetrahedral and octahedral sites of the spinel lattice, respectively. The relative areas of the subspectra in the Fe@Fe₃O₄ sample were 31% Fe(0), 16% FeOOH, and 53% Fe₃O₄. Since the area of each Mössbauer subspectrum can be related to the population of Fe atoms, assuming that the Lamb-Mössbauer factor is identical for all sites and compounds, the sample composition determined by Mössbauer spectroscopy coincides with that semi-quantitatively determined by X-ray diffraction. The spectrum of Pd/Fe@Fe₃O₄ (Fig. 6b) is formed by the FeOOH doublet, Fe(0) sextet, and two additional sextets with $H = 43.0$ T and 48.4 T that correspond to magnetite. The transformation of the magnetic field distribution in the Fe@Fe₃O₄ spectrum into the two well-defined sextets characteristic of magnetite indicates that the increase in temperature due to Pd²⁺ reduction, which occurs during sonication of the solution, is sufficient for the growth of nanoparticles. In contrast, a decrease from 31 to 11% in the area of the Fe(0) subspectrum and an increase from 16 to 33% in the area of the FeOOH subspectrum are observed. Therefore, it can be concluded that under these reaction conditions, Fe(0) is mainly oxidized to FeOOH. The mechanism of incorporation of Pd into the catalyst could be explained by the reduction of Pd²⁺ with Fe(0) on the surface, as well as by the coordination of the metal in solution with the exposed hydroxyl groups on the particle surface, followed by reduction by the Fe(0) that contains the core. Both processes can occur simultaneously.

Figure 6 Mössbauer spectra of **a** Fe@Fe₃O₄ and **b** Pd/Fe@Fe₃O₄.

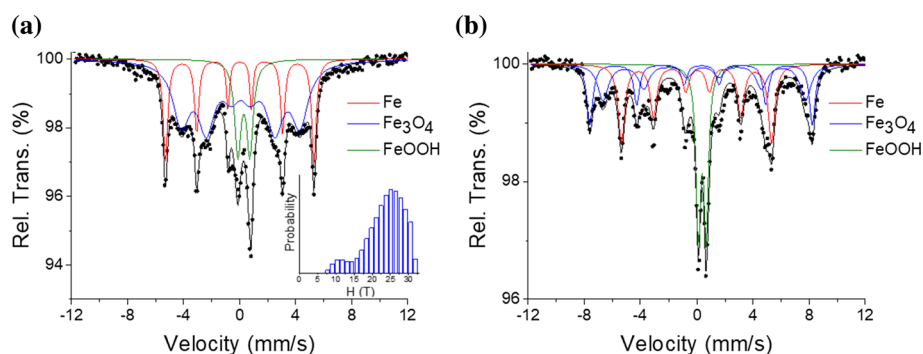
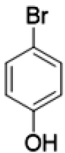
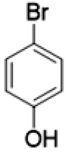
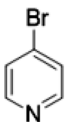


Table 1 Conversion (%) of Suzuki–Miyaura coupling reactions

Reactant		Reaction time (h)	Temperature (°C)	Conversion (%)	
				Bath	Inductor
	a	2	50	39	81
		4	50	51	85
		6	50	50	82
	a	4	30	47	70
		4	50	51	80
		4	70	60	85
	b	4	30	0	6
		4	70	25	70
		4	80	34	84

^a, ^bReaction conditions: **a** 4-bromophenol (1.8 mmol), phenylboronic acid (2.7 mmol), and 1,3,5-trimethoxybenzene (1.8 mmol), K₂CO₃ (3.6 mmol), 30 mg of Pd/Fe@FexOy (5 mol % Pd), in H₂O:EtOH (1:1), 10 ml. **b** 4-bromopyridine hydrochloride (1.8 mmol), phenylboronic acid (2.7 mmol), and 1,3,5-trimethoxybenzene (1.8 mmol), K₂CO₃ (7.2 mmol), 30 mg of Pd/Fe@FexOy (5 mol % Pd), in H₂O:EtOH (1:1), 10 ml. ¹H-NMR conversions were determined using 1,3,5-trimethoxybenzene as an internal standard, average of 3 independent reactions with 10% deviation

Suzuki–Miyaura coupling reactions

The Suzuki–Miyaura reaction was performed as a model to compare the efficiency obtained by thermal-bath heating and heating by magnetic induction. The temperature of the reaction solution was considered as the reaction temperature (see Figure S3).

To optimize the reaction time required for maximum conversion, aliquots of the mixture taken from the reaction of phenylboronic acid with 4-bromophenol at 50 °C were analyzed at 2, 4, and 6 h (Table 1). The results indicate that for both heating systems, there is a slight increase in the conversion with an increase in the reaction time from 2 to 4 h; however, after 4 h, a further increase in the reaction time to 6 h resulted in slight fluctuations in conversion, rather than progress. Based on these results, reactions **1a–b** were conducted over 4 h. The experiments were carried out three times, and the data are presented as the average of the independent reactions.

Table 1 shows the conversions of the coupling reactions between phenylboronic acid and 4-bromophenol and between phenylboronic acid and

4-bromopyridine as a function of the reaction temperature, using both heating methods.

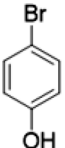
The data indicate that heating by means of a magnetic inductor results in higher conversions for both reactions compared to that achieved using thermal bath. An increase in the temperature results in a slight increase in the substrate conversion under thermal-bath and induction heating conditions. On average, for the reaction between phenylboronic acid and 4-bromophenol, 25–30% higher conversions were observed with magnetic induction heating compared to thermal-bath heating. Although the solution temperature was identical, induction produced a higher temperature on the surfaces of the nanoparticles. We can assume that the temperature on the nanoparticle surfaces increases by more than 40 °C by comparing the conversion achieved at 70 °C using a thermal bath with that achieved at 30 °C with magnetic induction heating. It has been demonstrated that the local heating of MNPs can generate a gradient of 45 °C at a distance of 0.5 nm from the surface of the MNPs in order to decay exponentially with distance [41]. Published studies suggest that reactions catalyzed by solid-supported Pd occur in solution owing to

leaching and subsequent redeposition of Pd [3]. Although we may assume that because of the increased temperature on the surface of the nanoparticles, where Pd is located, the reaction could occur superficially, we cannot rule out the possibility of some dissolution of Pd in the medium and subsequent redeposition. The temperature varies at a certain distance from the nanoparticles, but this decay is insignificant at a short distance. More precise experiments on the variation of temperature from the nanoparticles to the medium and the gradient in the concentration of Pd could provide insight into the mechanism. Regardless of the mechanism taking place, it is evident that the catalytic reaction occurs close enough to the particle surface for local heating to accelerate the reaction rate owing to the increase in temperature relative to the bulk solution. Although the reaction is temperature dependent, when the surfaces of the nanoparticles reach a certain temperature, an increase in the reaction-medium temperature does not considerably improve the conversion efficiency.

A relatively high conversion was achieved for the Suzuki–Miyaura coupling of phenylboronic acid and bromophenol, even at 30 °C, but the reaction with 4-bromopyridine requires a higher temperature; therefore, it does not occur at 30 °C in a thermal bath, and the yield obtained by magnetic induction heating is only 6% on average (Table 1). The conversions obtained at 70 and 80 °C for the reaction between phenylboronic acid and 4-bromopyridine heated by magnetic induction were 50% higher than those obtained at the same temperatures in a thermal bath (Table 1).

The heterogeneous Pd/Fe@Fe₃O₄ catalyst proved to be efficient in the Suzuki–Miyaura reactions

Table 2 Conversion achieved for the reaction between 4-bromophenol and phenylboronic acid performed during 4 h at 50 °C under magnetic field induction (223 kHz)

Reactant	Cycle	Conversion (%)
	1	81
	2	53
	3	32

*¹H-NMR conversions as average of 2 independent reactions with 8% deviation

studied, especially under magnetic induction heating. Subsequently, the reusability of the catalysts was assessed. Table 2 shows the evolution of the efficiency of the catalyst over three Suzuki–Miyaura coupling reaction cycles between phenylboronic acid and 4-bromophenol at 50 °C. Between each reaction cycle, the catalyst was recovered with a magnet, washed with distilled water and ethanol several times, and dried under vacuum.

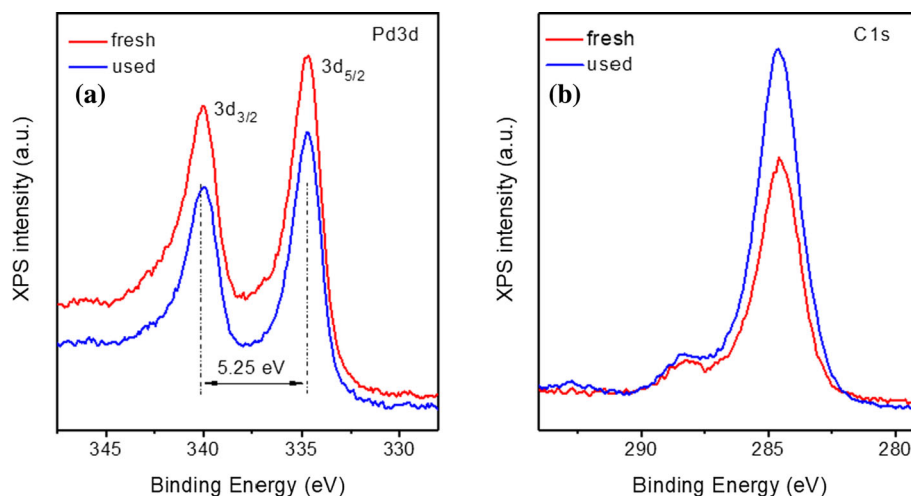
To determine the reason for the decrease in the reactivity of the catalyst in successive cycles, XPS measurements of the samples were carried out after reuse. Figure 7a, b compares the XPS spectra of Pd 3d and C 1 s corresponding to Pd/Fe@Fe₃O₄ fresh and reused samples. Note that the detailed XPS lineshape analysis reveals no significant differences between Fe 2p (not shown but similar to that displayed in Fig. 5a) and Pd 3d spectra in both samples. In addition, the Pd 3d spectrum includes more prominent asymmetric peaks with a minor contribution of surface native oxide, most likely because the surface of the nanoparticles is covered with a higher amount of C (see below), which reduces their exposure to air after preparation. The only difference between the spectra is the absolute emission intensity, in which signals are attenuated by the higher amount of C present on the surface. However, this modification did not change the relative surface atomic concentration ratio, suggesting low leaching of Pd. ICP-OES analysis of the catalyst revealed a slight variation in the composition of the MNPs with increased use; the Fe/Pd ratio changed by less than 5% after each cycle. In contrast, there exists a significant increase in the C concentration on the surface, which might be responsible of the poison effect observed in the catalytic behavior of the samples after use.

The loss in catalyst efficiency observed for Pd/Fe@Fe₃O₄ over three cycles is slightly greater than that reported for catalysts consisting of Pd supported on coated Fe₃O₄, such as Fe₃O₄/PEG/Pd [35] or Fe₃O₄/DA-Pd [22]. However, the use of uncoated magnetite offers the advantage of a facile and economical synthetic process.

Conclusions

We have shown that it is possible to perform Suzuki–Miyaura reactions under magnetic induction heating using Pd-functionalized MNPs without the addition

Figure 7 XPS (Al-K α) spectra of Pd/Fe@Fe₃O₄ fresh and reused. **a** Pd 3d core level, **b** C1 s core level of the catalyst.



of an organic coating, which saves time and resources and makes the process more sustainable.

Magnetic induction increases the efficiency of the catalytic process by approximately 25–35% compared to the reaction in which conventional heating was applied; this is due to the temperature on the surface of the MNPs being higher than that of the solvent. This allows the reaction to proceed without the need to heat the solvent to the required temperature. Furthermore, owing to the magnetic properties of the nanoparticles, the catalyst can be easily recovered and reused. However, further studies are required to increase the number of reaction cycles in which the recovered catalyst can be used.

Acknowledgements

We are grateful for financial support provided by the Government of Spain through project PGC2018-095642-B-I00. In addition, A. Villacampa and L. Duque acknowledge the Community of Madrid for Predoctoral contracts PEJD-2019-PRE/IND-15356 and PEJ-2019-AI/IND-12506, respectively, co-financed by the European Social Fund through the Youth Employment Operational Program and the Youth Employment Initiative (YEI).

Funding

Open Access funding provided thanks to the CRUE-CSIC agreement with Springer Nature.

Declarations

Conflict of interest The authors declare no conflict of interest.

Supplementary Information: The online version contains supplementary material available at <http://doi.org/10.1007/s10853-021-06591-w>.

Open Access This article is licensed under a Creative Commons Attribution 4.0 International License, which permits use, sharing, adaptation, distribution and reproduction in any medium or format, as long as you give appropriate credit to the original author(s) and the source, provide a link to the Creative Commons licence, and indicate if changes were made. The images or other third party material in this article are included in the article's Creative Commons licence, unless indicated otherwise in a credit line to the material. If material is not included in the article's Creative Commons licence and your intended use is not permitted by statutory regulation or exceeds the permitted use, you will need to obtain permission directly from the copyright holder. To view a copy of this licence, visit <http://creativecommons.org/licenses/by/4.0/>.

Supplementary Information: The online version contains supplementary material available at <http://doi.org/10.1007/s10853-021-06591-w>.

References

- [1] Cenini S, Gallo E, Caselli A et al (2006) Coordination chemistry of organic azides and amination reactions catalyzed by transition metal complexes. *Coord Chem Rev* 250:1234–1253
- [2] Hashmi ASK (2007) Gold-catalyzed organic reactions. *Chem Rev* 107:3180–3211
- [3] Yin L, Liebscher J (2007) Carbon-carbon coupling reactions catalyzed by heterogeneous palladium catalysts. *Chem Rev* 107:133–173
- [4] Kuninobu Y, Takai K (2011) Organic reactions catalyzed by rhenium carbonyl complexes. *Chem Rev* 111:1938–1953
- [5] Hernández JG, Friščić T (2015) Metal-catalyzed organic reactions using mechanochemistry. *Tetrahedron Lett* 56:4253–4265
- [6] Nájera C, Beletskaya IP, Yus M (2019) Metal-catalyzed regioselective organic reactions. *Chem Soc Rev* 48:4515–4618
- [7] Cheng WM, Shang R (2020) Transition metal-catalyzed organic reactions under visible light: recent developments and future perspectives. *ACS Catal* 10:9170–9196
- [8] Miyaura N, Yamada K, Suzuki A (1979) A new stereospecific cross-coupling by the palladium-catalyzed reaction of 1-alkenylboranes with 1-alkenyl or 1-alkynyl halides. *Tetrahedron Lett* 20:3437–3440. [https://doi.org/10.1016/S0040-4039\(01\)95429-2](https://doi.org/10.1016/S0040-4039(01)95429-2)
- [9] Hayler JD, Leahy DK, Simmons EM (2019) A pharmaceutical industry perspective on sustainable metal catalysis. *Organometallics* 38:36–46. <https://doi.org/10.1021/acs.organo.8b00566>
- [10] Das P, Bora U, Tairai A, Sharma C (2010) Triphenylphosphine chalcogenides as efficient ligands for room temperature palladium(II)-catalyzed Suzuki–Miyaura reaction. *Tetrahedron Lett* 51:1479–1482. <https://doi.org/10.1016/j.tlet.2010.01.032>
- [11] Climent MJ, Corma A, Iborra S, Mifsud M (2007) Heterogeneous palladium catalysts for a new one-pot chemical route in the synthesis of fragrances based on the heck reaction. *Adv Synth Catal* 349:1949–1954. <https://doi.org/10.1002/ADSC.200700026>
- [12] Chen Y, Wang M, Zhang L et al (2017) Poly(*o*-aminothiophenol)-stabilized Pd nanoparticles as efficient heterogeneous catalysts for Suzuki cross-coupling reactions. *RSC Adv* 7:47104–47110. <https://doi.org/10.1039/c7ra09947a>
- [13] Rahimi L, Mansoori Y, Nuri A, Esquivel D (2020) A new magnetically retrievable porous supported catalyst for the Suzuki–Miyaura cross-coupling reaction. *ChemistrySelect* 5:11690–11697. <https://doi.org/10.1002/slct.202003198>
- [14] Martin R, Buchwald SL (2008) Palladium-catalyzed Suzuki–Miyaura cross-coupling reactions employing dialkylbiaryl phosphine ligands. *Acc Chem Res* 41:1461–1473
- [15] Fihri A, Bouhrara M, Nekoueshahraki B et al (2011) Nanocatalysts for Suzuki cross-coupling reactions. *Chem Soc Rev* 40:5181–5203. <https://doi.org/10.1039/c1cs15079k>
- [16] Veisi H, Amini Manesh A, Eivazi N, Faraji AR (2015) Palladium nanoparticles supported on 1,3-dicyclohexylguanidine functionalized mesoporous silica SBA-15 as highly active and reusable catalyst for the Suzuki–Miyaura cross-coupling reaction. *RSC Adv* 5:20098–20107. <https://doi.org/10.1039/c4ra14668a>
- [17] Zheng Z, Li H, Liu T, Cao R (2010) Monodisperse noble metal nanoparticles stabilized in SBA-15: synthesis, characterization and application in microwave-assisted Suzuki–Miyaura coupling reaction. *J Catal* 270:268–274. <https://doi.org/10.1016/j.jcat.2010.01.004>
- [18] Rohani S, Mohammadi Ziarani G, Badii A et al (2019) Mesoporous hierarchically hollow flower-like CoAl-LDH@N, S-doped Graphene@Pd nanoarchitectures for Heck couplings. *Catal Lett* 149:2984–2993. <https://doi.org/10.1007/s10562-019-02880-x>
- [19] Sokolov VI, Rakov EG, Bumagin NA, Vinogradov MG (2010) New method to prepare nanopalladium clusters immobilized on carbon nanotubes: a very efficient catalyst for forming carbon-carbon bonds and hydrogenation. *Fuller Carbon Nanostructures* 18:558–563. <https://doi.org/10.1080/1536383X.2010.488077>
- [20] Llabrés i Xamena FX, Abad A, Corma A, Garcia H (2007) MOFs as catalysts: activity, reusability and shape-selectivity of a Pd-containing MOF. *J Catal* 250:294–298. <https://doi.org/10.1016/j.jcat.2007.06.004>
- [21] Augustyniak AW, Zawartka W, Navarro JAR, Trzeciak AM (2016) Palladium nanoparticles supported on a nickel pyrazolate metal organic framework as a catalyst for Suzuki and carbonylative Suzuki couplings. *Dalt Trans* 45:13525–13531. <https://doi.org/10.1039/c6dt02242a>
- [22] Long Y, Liang K, Niu J et al (2015) Agglomeration of Pd0 nanoparticles causing different catalytic activities of Suzuki carbonylative cross-coupling reactions catalyzed by PdII and Pd0 immobilized on dopamine-functionalized magnetite nanoparticles. *New J Chem* 39:2988–2996. <https://doi.org/10.1039/c4nj02285h>
- [23] Bobb JA, Ibrahim AA, El-Shall MS (2018) Laser synthesis of carbonaceous TiO₂ from metal-organic frameworks: optimum support for Pd nanoparticles for C–C cross-coupling reactions. *ACS Appl Nano Mater* 1:4852–4862. <https://doi.org/10.1021/acsanm.8b01045>
- [24] Yoon TJ, Lee W, Oh YS, Lee JK (2003) Magnetic nanoparticles as a catalyst vehicle for simple and easy

- recycling. *New J Chem* 27:227–229. <https://doi.org/10.1039/b209391j>
- [25] Shylesh S, Wang L, Demeshko S, Thiel WR (2010) Facile synthesis of mesoporous magnetic nanocomposites and their catalytic application in carbon–carbon coupling reactions. *ChemCatChem* 2:1543–1547. <https://doi.org/10.1002/cctc.201000215>
- [26] Ahmadi A, Sedaghat T, Motamedi H, Azadi R (2020) Anchoring of Cu (II)-Schiff base complex on magnetic mesoporous silica nanoparticles: catalytic efficacy in one-pot synthesis of 5-substituted-1H-tetrazoles, antibacterial activity evaluation and immobilization of α -amylase. *Appl Organomet Chem* 34:e5572. <https://doi.org/10.1002/aoc.5572>
- [27] Rafiee E, Kahrizi M, Joshaghani M, Ghaderi-Sheikhi Abadi P (2016) New strategy by a two-component heterogeneous catalytic system composed of Pd–PVP–Fe and heteropoly acid as co-catalyst for Suzuki coupling reaction. *Res Chem Intermed* 42:5573–5585. <https://doi.org/10.1007/s11164-015-2387-5>
- [28] Esmaeilpour M, Zahmatkesh S, Fahimi N, Nosratabadi M (2018) Palladium nanoparticles immobilized on EDTA-modified Fe₃O₄@SiO₂ nanospheres as an efficient and magnetically separable catalyst for Suzuki and Sonogashira cross-coupling reactions. *Appl Organomet Chem* 32:e4302. <https://doi.org/10.1002/aoc.4302>
- [29] Li XQ, Zhang WX (2006) Iron nanoparticles: the core-shell structure and unique properties for Ni(II) sequestration. *Langmuir* 22:4638–4642. <https://doi.org/10.1021/la060057k>
- [30] Macdonald JE, Kelly JA, Veinot JGC (2007) Iron/iron oxide nanoparticle sequestration of catalytic metal impurities from aqueous media and organic reaction products. *Langmuir* 23:9543–9545. <https://doi.org/10.1021/la7011827>
- [31] Macdonald JE, Veinot JGC (2008) Removal of residual metal catalysts with iron/iron oxide nanoparticles from coordinating environments. *Langmuir* 24:7169–7177. <https://doi.org/10.1021/la8006734>
- [32] Ceylan S, Friese C, Lammel C et al (2008) Inductive heating for organic synthesis by using functionalized magnetic nanoparticles inside microreactors. *Angew Chemie Int Ed* 47:8950–8953. <https://doi.org/10.1002/anie.200801474>
- [33] Meffre A, Mehdaoui B, Connord V et al (2015) Complex nano-objects displaying both magnetic and catalytic properties: a proof of concept for magnetically induced heterogeneous catalysis. *Nano Lett* 15:3241–3248. <https://doi.org/10.1021/acs.nanolett.5b00446>
- [34] Phenrat T, Kumloet I (2016) Electromagnetic induction of nanoscale zerovalent iron particles accelerates the degradation of chlorinated dense non-aqueous phase liquid: Proof of concept. *Water Res* 107:19–28. <https://doi.org/10.1016/j.watres.2016.10.035>
- [35] De Cattelle A, Billen A, Brulot W et al (2019) Magnetically induced Suzuki and Sonogashira reaction performed using recyclable, palladium-functionalized magnetite nanoparticles. *J Organomet Chem* 899:120905. <https://doi.org/10.1016/j.jorganchem.2019.120905>
- [36] Zhou S, Johnson M, Veinot JGC (2010) Iron/iron oxide nanoparticles: a versatile support for catalytic metals and their application in Suzuki–Miyaura cross-coupling reactions. *Chem Commun* 46:2411–2413. <https://doi.org/10.1039/b922462a>
- [37] Brand RA (1987) Improving the validity of hyperfine field distributions from magnetic alloys. *Nucl Instrum Methods Phys Res Sect B Beam Interact Mater Atoms* 28:398–416. [https://doi.org/10.1016/0168-583X\(87\)90182-0](https://doi.org/10.1016/0168-583X(87)90182-0)
- [38] Biesinger MC, Payne BP, Grosvenor AP et al (2011) Resolving surface chemical states in XPS analysis of first row transition metals, oxides and hydroxides: Cr, Mn, Fe, Co and Ni. *Appl Surf Sci* 257:2717–2730. <https://doi.org/10.1016/J.APSUSC.2010.10.051>
- [39] Rubio-Zuazo J, Chainani A, Taguchi M et al (2018) Electronic structure of FeO, γ -Fe₂O₃, and Fe₃O₄ epitaxial films using high-energy spectroscopies. *Phys Rev B*. <https://doi.org/10.1103/PhysRevB.97.235148>
- [40] Cui H, Wang L, Shi M, Li Y (2017) Morphology and phase control of iron oxide polymorph nanoparticles. *Mater Res Express* 4:045006. <https://doi.org/10.1088/2053-1591/AA680D>
- [41] Riedinger A, Guardia P, Curcio A et al (2013) Subnanometer local temperature probing and remotely controlled drug release based on Azo-functionalized iron oxide nanoparticles. *Nano Lett* 13:2399–2406. <https://doi.org/10.1021/nl400188q>

Publisher's Note Springer Nature remains neutral with regard to jurisdictional claims in published maps and institutional affiliations.